JUSTC

Article

http://justc.ustc.edu.cn

Received: September 14, 2024; Accepted: December 02, 2024

Preliminary solution to parameters for WFST

Yuxi Jiang[1,2], Fan Li[1] ✉, Jian Chen[1], Bin Li[1], Tianrui Sun[1], Yantian Zhu[1], and Xin Wang[1,2] ✉

[1]*Purple Mountain Observatory, Chinese Academy of Sciences, Nanjing 210023, China;*
[2]*School of Astronomy and Space Science, University of Science and Technology of China, Hefei 230026, China*

✉Correspondence: Fan Li, E-mail: lifan@pmo.ac.cn; Xin Wang, E-mail: wangxin@pmo.ac.cn

Graphical abstract

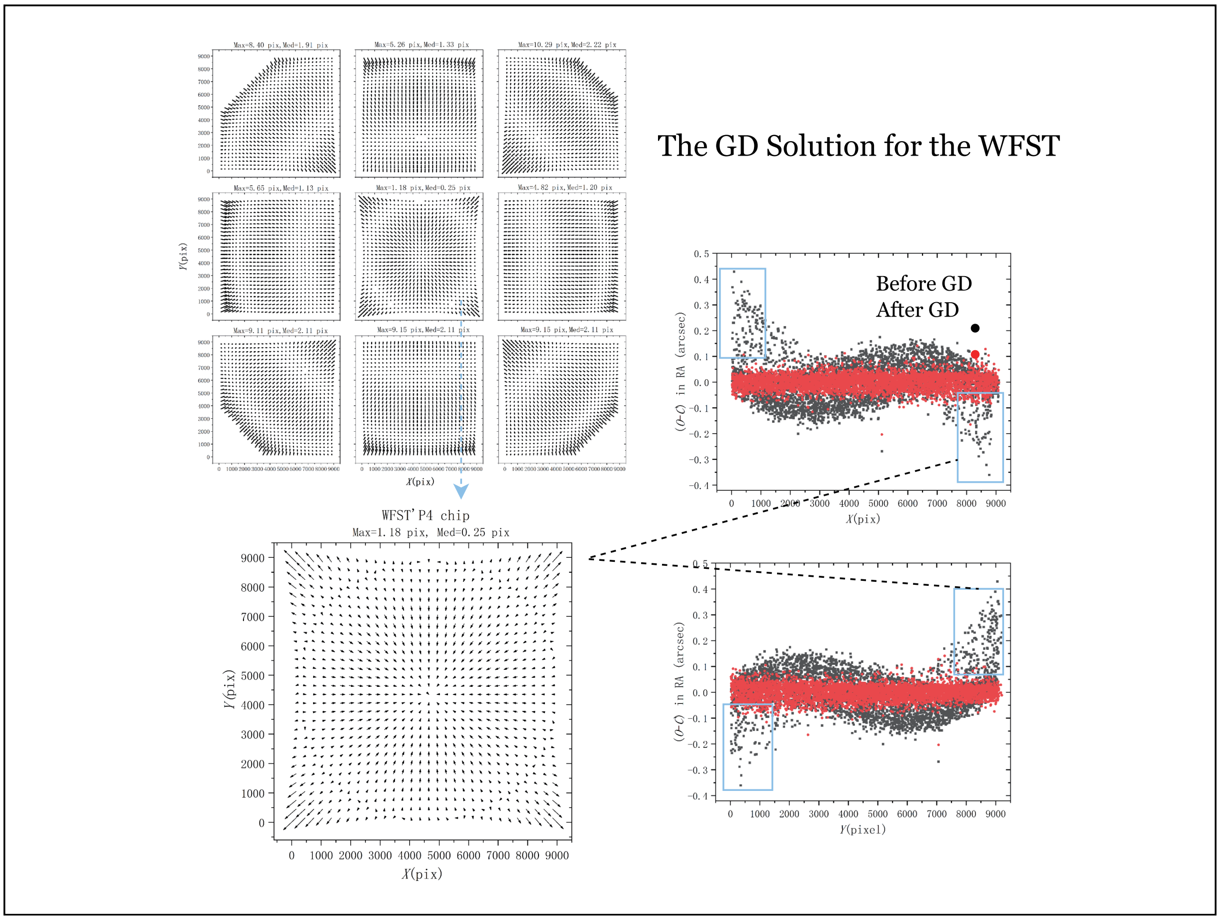

After geometric distortion (GD) correction in the WFST, the residuals are significantly reduced, especially at the CCD edges.

Public summary

- The geometric distortion (GD) solutions show maximum distortions between 1.18 and 10.29 pixels for the Wide Field Survey Telescope (WFST) chips, with central chips exhibiting lower distortion.
- The precision of the WFST reaches 4 mas after applying the GD correction.
- The interchip gaps of the WFST range from 1.922 mm to 7.765 mm, corresponding to 10 μm/pixel, aligning with the design and measurements.

Citation: Jiang Y X, Li F, Chen J, et al. Preliminary solution to parameters for WFST. *JUSTC*, **2025**, 55(4): 0402. CSTR: 32290.14.JUSTC-2024-0124.
DOI: 10.52396/JUSTC-2024-0124

JUSTC

Article

http://justc.ustc.edu.cn

Received: September 14, 2024; Accepted: December 02, 2024

Preliminary solution to parameters for WFST

Yuxi Jiang[1,2], Fan Li[1] ✉, Jian Chen[1], Bin Li[1], Tianrui Sun[1], Yantian Zhu[1], and Xin Wang[1,2] ✉

[1]*Purple Mountain Observatory, Chinese Academy of Sciences, Nanjing 210023, China;*
[2]*School of Astronomy and Space Science, University of Science and Technology of China, Hefei 230026, China*

✉Correspondence: Fan Li, E-mail: lifan@pmo.ac.cn; Xin Wang, E-mail: wangxin@pmo.ac.cn

Cite This: *JUSTC*, **2025**, 55(4): 0402 (9pp)

Read Online

Abstract: The Wide Field Survey Telescope (WFST) is located at 4200 m on Saishiteng Mountain in Lenghu, Qinghai Province, China. It features a primary mirror with a diameter of 2.5 m and a camera equipped with nine CCDs, providing a wide field of view of approximately 3×3 square degrees. Calibration parameters are essential to ensure the precision of astrometric observations with the WFST. These parameters are derived from geometric distortion (GD) and gaps through astrometric modeling and are subsequently validated via the Yao'An High Precision Telescope (YAHPT). The GD solutions show maximum distortions between 1.18 and 10.29 pixels for the WFST chips, with central chips exhibiting lower distortion. After applying the GD correction, the precision of the WFST reaches 4 mas. The interchip gaps of the WFST range from 1.922 mm to 7.765 mm, corresponding to 10 μm/pixel, aligning with the design and measurements. The calibrated parameters guarantee that the WFST can perform highly accurate astrometric measurements. Furthermore, as the WFST undergoes updates, the parameter model remains consistently applicable.

Keywords: astronomical instrumentation; astrometry; astronomy data analysis; astronomy data reduction; image processing

CLC number: P122 **Document code:** A

1 Introduction

The Wide Field Survey Telescope (WFST) was jointly built by the University of Science and Technology of China (USTC) and the Purple Mountain Observatory (PMO). It is located at an altitude of 4200 m above sea level on Saishiteng Mountain in Lenghu, Qinghai Province, China. Research[1] indicates that 70% of the nights in Lenghu have clear, photometric conditions, with a median seeing of 0.75". The WFST has a primary mirror with a diameter of 2.5 m and a camera consisting of nine CCDs, each offering a resolution of 9k×9k pixels in the main focal plane. With these specifications, the WFST provides a effective field of view of approximately 6.5 square degrees[2].

The WFST is equipped with six filters (*u*, *g*, *r*, *i*, *z*, and *w*) and focuses its observations primarily on the northern hemisphere. The "*w*" is a white filter, and it is sensitive for detecting asteroids in the solar system. With an exposure of 30 s, the WFST can achieve magnitudes of 22.27, 23.32, 22.84, and 22.31 in the AB magnitude system for the respective bands[2]. As of April 8, 2024, the WFST identifies 11 new near-Earth asteroids[3–5]. Future observations contribute to the astrometric study of asteroid ephemerides and planetary physical properties[6–9].

Astrometric requirements for the WFST necessitate the precise measurement of its calibration parameters. Proper calibration minimizes systematic errors and enhances the precision of positional data, which is fundamental for WFST. As the WFST undergoes updates, the same model for determining these calibration parameters is consistently applied, ensuring high precision in astrometric performance across various phases. In addition, the Yao'An High Precision Telescope (YAHPT) is a telescope designed for high-precision astrometry[10–17], and the parameter model used to calibration can be validated through its measurements.

The YAHPT is located at Yao'An Station in Yunnan Province and features an 80 cm primary mirror diameter. Equipped with a PI CCD camera with a resolution of 2k×2k, the telescope offers an effective field of view of 11.8' ×11.8'. Additionally, the YAHPT is equipped with Johnson filters covering the B, V, Rc, and Ic bands. Table 1 summarizes the key specifications of the two telescopes.

Numerous studies have explored the calibration of astrometric parameters, providing valuable insights that can inform data preprocessing and enhance telescope calibration accuracy in practice. Guo et al.[12] analyzed the astrometric accuracy in three aspects: CCD geometric distortion (GD), limiting magnitude, and astrometric performance when observing fast-moving faint objects. Their findings indicated that YAHPT maintains a stable GD solution, which can provide accurate target positions even in scenarios where calibration stars (< 20) are in a sparse star field.

Table 1. Key specifications of WFST and YAHPT.

Telescope	WFST	YAHPT
Focal ratio	$f/2.48$	$f/10$
Diameter of primary mirror	250 cm	80 cm
Size of CCD array	9216×9232	2048×2048
CCD field of view	3°×3°	11.8'×11.8'
Angular resolution	0.332 arcsec/pixel	0.347 arcsec/pixel

CSTR: 32290.14.JUSTC-2024-0124
DOI: 10.52396/JUSTC-2024-0124
JUSTC, **2025**, 55(4): 0402

The GD as a calibration parameter has been shown to have an impact on the astrometric accuracy, prompting extensive research in this field. In 2003, Anderson et al.[18] improved the accuracy of WFPC2 on the HST by correcting for the GD. In subsequent studies, Anderson et al.[19] and Bellini et al.[20] used a self-calibration method to solve the GD effects found on the European Southern Observatory (ESO) 2.2 m telescope in 2006 and the Large Binocular Telescope (LBT) in 2010. These adjustments resulted in precisions of 7 milliarcseconds (mas) and 15 mas. In 2019, Wang et al.[21] applied two third-order polynomial fits and a lookup table to obtain GD corrections via Gaia DR2. These corrections are applied to a 2.3 m Bok telescope, which is composed of four chips, for the Beijing-Arizona Sky Survey (BASS). The corrections lead to a precision of approximately 20 mas for bright stars. Zheng et al.[22] also used differential astrometry and photographic astrometry, deriving the distortions of the chips and the relative positions between them via Gaia DR3. This method is able to reduce the propagation of errors due to residual distortions. When a wide-field telescope with photographic astrometry is employed, a polynomial fit to the celestial coordinates and the pixel coordinates yields excessive residuals, rendering the calculated distortions implausible[23]. It has been demonstrated that the CCD chip gaps fluctuate over time owing to the instrumental effects of the telescope. Using photographic astrometry methods to determine the gaps between chips, it is possible to improve the precision[20,23].

This paper utilizes the model of an astrometric telescope to calibrate the WFST astrometric parameters from two distinct perspectives. A six-constant model was developed to calculate the projected standard coordinates and the pixel coordinates on the basis of the positions of the catalogs. Notably, the excess is a geometric distortion. We calculate the WFST distortion values from photographic astrometry. Furthermore, the WFST is composed of nine chips, necessitating the consideration and calculation of the interchip gap as an integral aspect of the astrometric parameters. The paper is organized as follows. Section 2 evaluates the calibrated parameters of the WFST with observations, including the GD and gaps. Section 3 of the paper provides a summary.

2 Calibration parameters for WFST

2.1 Observations

The parameters are calibrated in an astrometry solution on the basis of observational data from the WFST. Additionally, data from the YAHPT are used to validate our model. We use 70 images taken by WFST on November 18, 2023, and 27 images of M35 captured by YAHPT on January 1, 2022, as detailed in Table 2. All CCD images are preprocessed for bias and flat corrections. All sources within each image are subsequently scanned with SExtractor[24] to acquire the pixel coordinates. The WFST uses data from the Ecliptic Survey, with the observed sky area distributed as illustrated in Fig. 1. The right ascension spans from 60°.285 to 155°.417, and the declination ranges from 13°.464 to 33°.085.

The stars in the images are matched via Gaia DR3[25] as a calibration catalog. Positions from Gaia are transformed to topocentric positions by taking into account proper motion, annual aberration, parallax, and atmospheric refraction. This process ensures that each star in the image has corresponding pixel coordinates and celestial sphere coordinates.

Table 2. The observations of WFST and YAHPT.

Telescope	Obs. date (y-m-d)	Frames	Filter	Exptime (s)	ZD (mean) (°)	HA (mean) (h)
WFST	2023-11-18	70	W	60	23–42(31.3)	−2.6 – +2.6(0.42)
YAHPT	2022-01-01	27	I	50	26–32(29.7)	−2.4 – +1.9(−2.1)

ZD and HA refer to the zenith distance range and the hour-angle range of the observations.

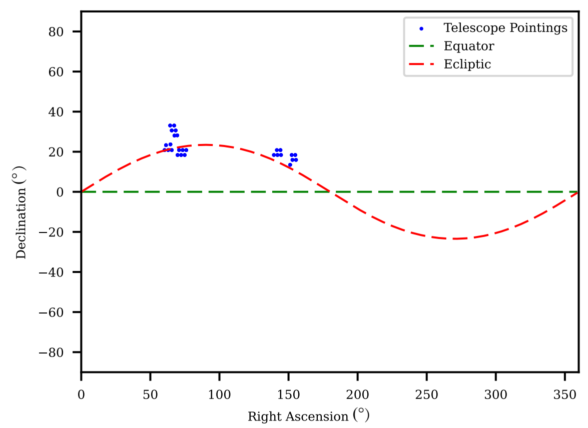

Fig. 1. WFST observations from the Ecliptic Survey from 2023-10-18, with the blue points indicating the telescope's position. The red and green dotted lines represent the equator and ecliptic, respectively.

2.2 Geometric distortion

The telescope's GD is derived by performing a six-constant model (linear transformation) that calculates the projection from catalog positions to standard and pixel coordinates. The distortion is quantified as the residuals in position after applying this transformation. Recently, Zheng et al.[22] applied differential astrometry to solve for GD. For fainter stars that cannot be identified in the Gaia catalog, their method relies solely on the pixel coordinates of stars detected on the CCD. In our observations of the WFST, we employ the method of photographic astrometry as described by Ref. [22], as there are an adequate number of stars available for use as calibration stars.

In photographic astrometry, if the CCD is considered without distortion, the pixel coordinates of each star on the CCD image should conform to the four-constant model relationship with its standard coordinates. In 2003, for a small field of view of the telescope, Anderson et al.[18] suggested that the frame without any distortion was to be: If the star positions defining it have been corrected in such a way that the positions of the same stars, measured in any image with a different pointing but corrected in the same way, can be transformed into those of this frame with nothing more than a displacement, a rotation, and a scale factor. Considering the uncertainty of the star catalog, Anderson et al. employed the self calibration method to measure the GD of the Hubble Space Telescope. Since the stars do not exhibit significant

CSTR: 32290.14.JUSTC-2024-0124
DOI: 10.52396/JUSTC-2024-0124
JUSTC, **2025**, 55(4): 0402

movement at night, a dense field is obtained by shifting the telescope, which is then utilized to resolve the distortion within the telescope. After 2022, the accuracy of the star positions in Gaia DR3[25] is significantly higher than that of ground-based telescopes, allowing the projected standard coordinates from Gaia DR3 to be directly referenced as an absolutely accurate system. In our calculation of the GD, we directly obtain the positions of stars in the Gaia DR3[25] catalog within the observed sky region on the basis of the known orientation of the telescope. These positions are then used to derive the projected standard coordinates as a reference.

Multiple observations are used to derive the GD during the same night. After initial processing to acquire the celestial coordinates of the point source, standard coordinates on the tangent plane are obtained via gnomonic projection. The six-constant model is then used directly to fit the standard and pixel coordinates via least squares, resulting in a residual $(O-C)_s$ for each star.

It is recommended that the GD of the YAHPT be solved prior to the WFST, as it can serve to demonstrate the validity of the method. For the YAHPT, the selection of a primary coordinate system is regarded as a preliminary step. The pixel coordinates are partitioned into 25 grids, each measuring 410×410 pixels. For the WFST, the GD is calculated for each chip separately. The pixel coordinates are partitioned into 900 grids, each with a size of 300×300 pixels. Typically, there are approximately 100 stars in each grid. The residuals of the stars within each grid are averaged to determine the residuals of the grid. The position of the grid is determined by the location of its central pixel. The residuals in each grid are averaged, and the remaining systematic residuals are then used to derive the GD. The residuals after GD correction exhibit a random distribution, indicating that systematic errors have been effectively corrected. After normalizing the coordinates, we apply a fourth-order polynomial fit to the grid positions and residuals via the least-squares method to obtain the polynomial coefficients.

$$\begin{aligned}\Delta x = {} & a_0+a_1x+a_2y+a_3x^2+a_4xy+a_5y^2+\\ & a_6x^3+a_7x^2y+a_8xy^2+a_9y^3+a_{10}x^4+\\ & a_{11}x^3y+a_{12}x^2y^2+a_{13}xy^3+a_{14}y^4,\\ \Delta y = {} & b_0+b_1x+b_2y+b_3x^2+b_4xy+b_5y^2+\\ & b_6x^3+b_7x^2y+b_8xy^2+b_9y^3+b_{10}x^4+\\ & b_{11}x^3y+b_{12}x^2y^2+b_{13}xy^3+b_{14}y^4,\end{aligned} \tag{1}$$

where Δx and Δy are residuals after the six-constant model. These coefficients are subsequently used to correct the original pixel coordinates (x_0, y_0). The process of correcting coordinates involves fitting the GD-corrected coordinates with the standard coordinates (ξ,η) to compute the residuals. These residuals are then averaged and the process is repeated for approximately 5 iterations until the residuals of the polynomial solution converge. This iterative approach minimizes systematic residuals in the data and enhances the accuracy of the correction.

The GD solution for a single night of WFST observations shows a higher average GD value for the outer chips and a lower GD value for the central chip, which is consistent with the optical design (based on internal report data). We select stars in the magnitude range of 16.5−20 for distortion correction, as stars brighter than 16.5 tend to be oversaturated in the CCD. For the chip P4, the maximum distortion reaches 1.18 pixels, with an average of 0.25 pixels (see Fig. 2), and the residuals' distribution after distortion correction is randomized (see Fig. 3). The residuals and standard deviations of the corrected right ascension and declination are presented separately in Fig. 4 and Fig. 5. After applying the GD correction, the residues are generally reduced to within 10 mas. As a result, the astrometric precision of the WFST has improved, with the median standard deviation reaching approximately 4 mas.

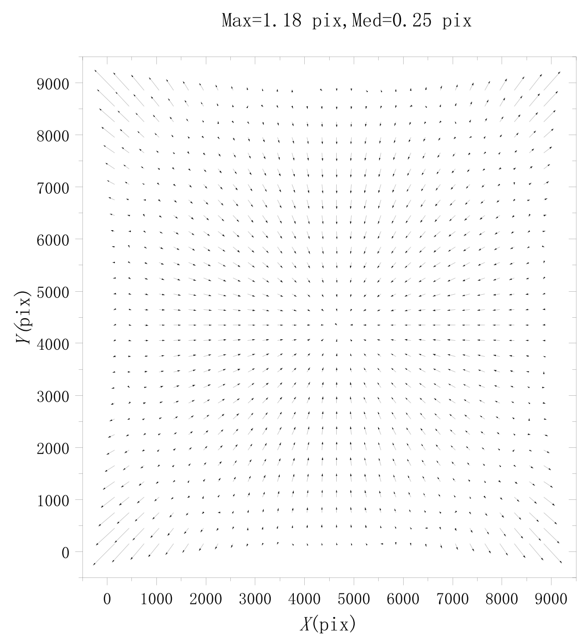

Fig. 2. Geometric distortion (GD) for WFST'P4. The magnitude of each vector is exaggerated by a factor of 500.

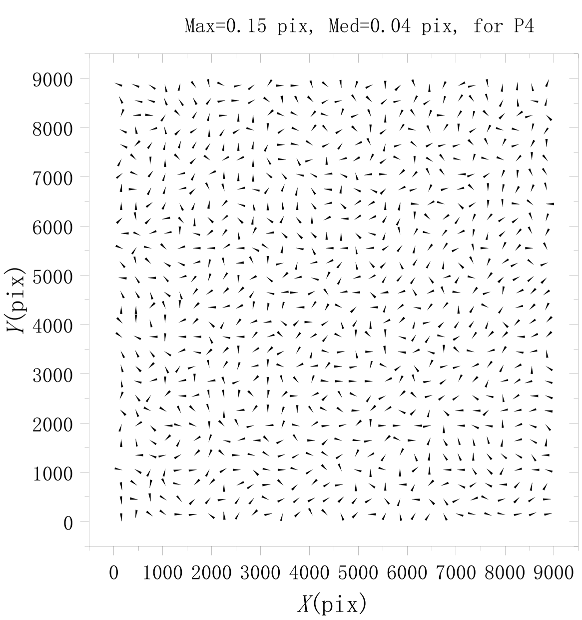

Fig. 3. The remaining residuals' distributions after distortion correction for P4. The magnitude of each vector is exaggerated by a factor of 1000.

CSTR: 32290.14.JUSTC-2024-0124
DOI: 10.52396/JUSTC-2024-0124
JUSTC, **2025**, 55(4): 0402

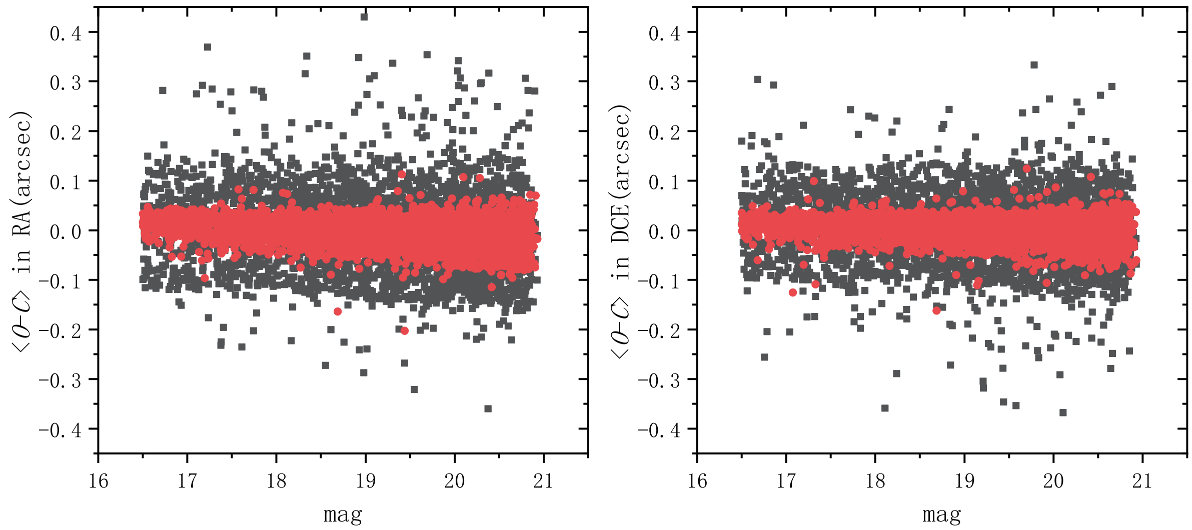

Fig. 4. The distribution of residuals for P4 is shown, with the red points representing residuals after distortion correction and the black points indicating residuals before distortion correction.

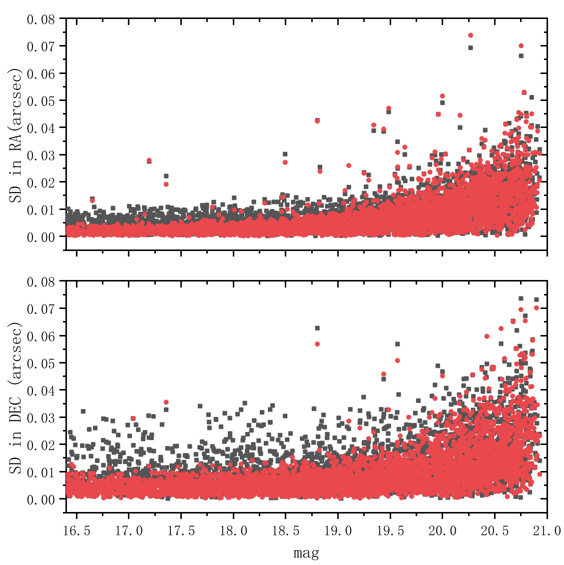

Fig. 5. The distribution of standard deviations (SDs) for P4 is shown, with the red points representing SDs after distortion correction and the black points indicating SDs before distortion correction. Applying GD correction reduced the median SD from 6.45 mas to 4.62 mas in RA for P4.

We also use the same method to solve the GD for other chips (see Fig. 6 and Fig. 7). Fig. 8 shows the change in standard deviation before and after GD correction for all chips. The implementation of distortion correction notably enhances the accuracy of each chip.

We also solve the GD solution for one night of the YAHPT telescope, which is similar to the GD value solved for the YAHPT by previous studies[12], with a maximum distortion value of approximately 0.66 pixels (see Fig. 9). We use the residuals and grid coordinates from 25 grids to derive a distorted polynomial. To more intuitively display the distortion distribution, we increase the number of grids to 225, adding more grid coordinates, which, in combination with the polynomial, results in distortion offsets. The distribution of residuals for the YAHPT is shown in Fig. 10. These residuals are smaller than those when only the six-constant model.

2.3 Measurement of chip gaps

As a crucial calibration parameter, the size of the gaps is also calculated in the astrometry solution. The chip gap in the Bok telescope is calculated via photographic astrometry, specifically by designating a chip as the primary coordinate and determining the position of selected points on other chips relative to that chip, using standard coordinates in between for the connection[22]. WFST, which has 9 chips and 12 gaps (see Fig. 11). For each gap, we select two chips adjacent to it, one chip is chosen as the primary coordinate, and the pixel coordinates of the points close to the gap are known to be connected by the standard coordinates of the stars on the two chips. We select a fourth-order polynomial for the plate model[21]. Extrapolating its position from the fourth-order polynomial may lead to inaccuracies if we choose a point distant from the main coordinate chip.

Therefore, we directly select 100 points near the edge of each chip, employ a polynomial to determine their standard coordinates, and subsequently fit a straight line to these 100 points to ascertain the size and parallelism of the gap in the standard coordinates. For instance, consider the gap between chips P0 and P1. Chip P0 has a size of 9216×9232, whereas chip P2 has a size of 9232×9216. On the basis of the gap's position, the horizontal coordinate of the point adjacent to the gap in chip P0 is 9215.5. For the vertical coordinate system, 100 points ranging from 100 to 9000 are selected. Chip P1 maintains a horizontal coordinate of 0.5 for all points near the gap, with the vertical coordinate ranging from 100 to 9000 across 100 points. After the pixel coordinates of the points are selected, their standard coordinates are determined by inputting their pixel coordinates into the plate model corresponding to the chip where they are located. In conclusion, the gap and parallelism are determined by fitting 100 points from the two chips. Table 3 illustrates the gaps between the 9 chips, totaling 12 gaps. The gap between chip P4 and chip P7 is the widest, averaging 7.7 mm, which corresponds to 10 μm/pixel.

CSTR: 32290.14.JUSTC-2024-0124
DOI: 10.52396/JUSTC-2024-0124
JUSTC, **2025**, 55(4): 0402

This value is close to the telescope's design specification of 7.9 mm, as indicated in the internal report data.

The pixel coordinates of the projection center can be accurately derived from the gaps, which remain constant throughout the solution process. We examine three cases: (a) The projection center is the point of each chip and the center

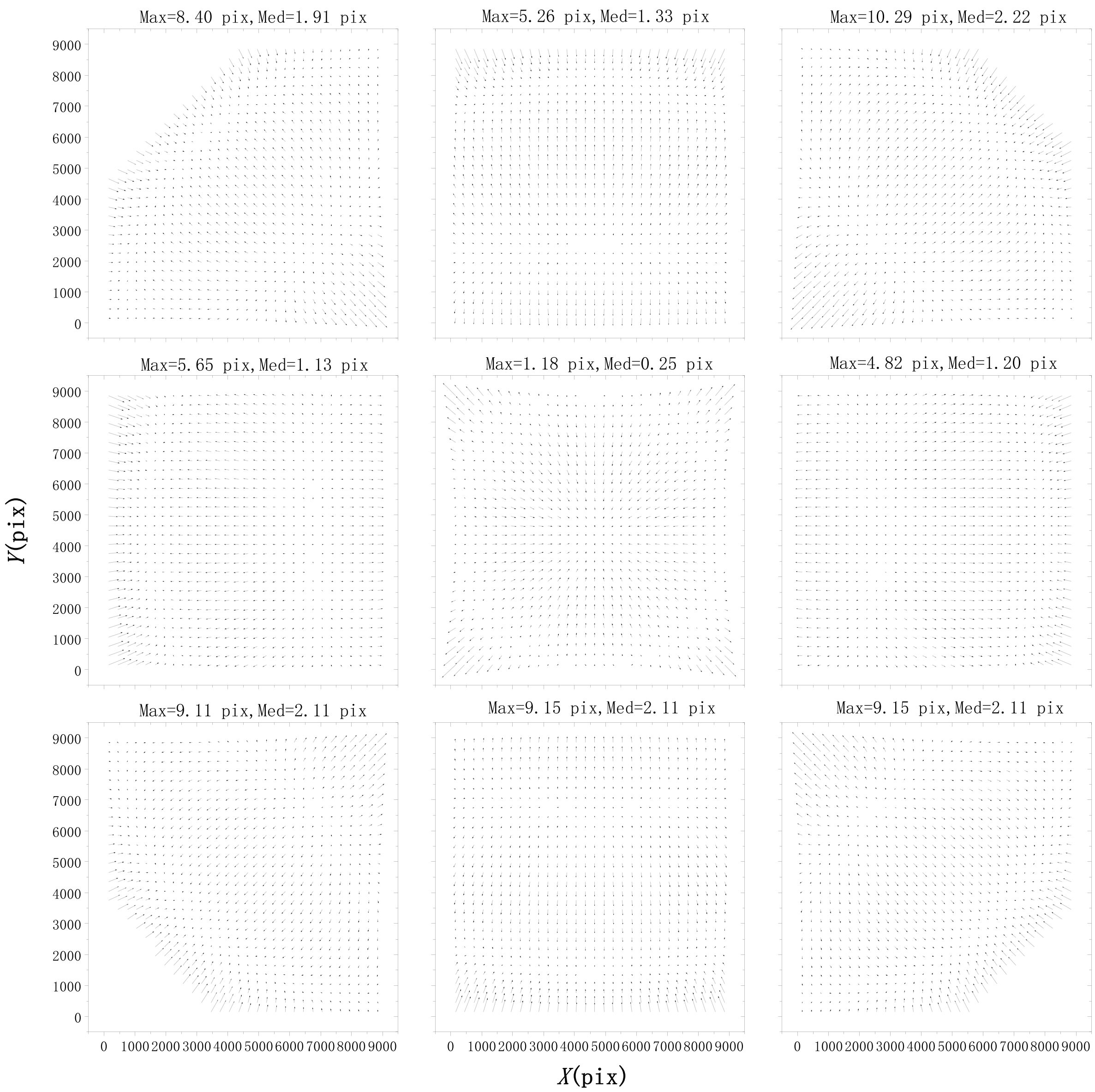

Fig. 6. Geometric distortion (GD) for the WFST. The magnitude of each vector is scaled by a factor of 50 for P0, P2, P6, and P8; by a factor of 100 for P1, P3, P5, and P7; and by a factor of 1000 for P4.

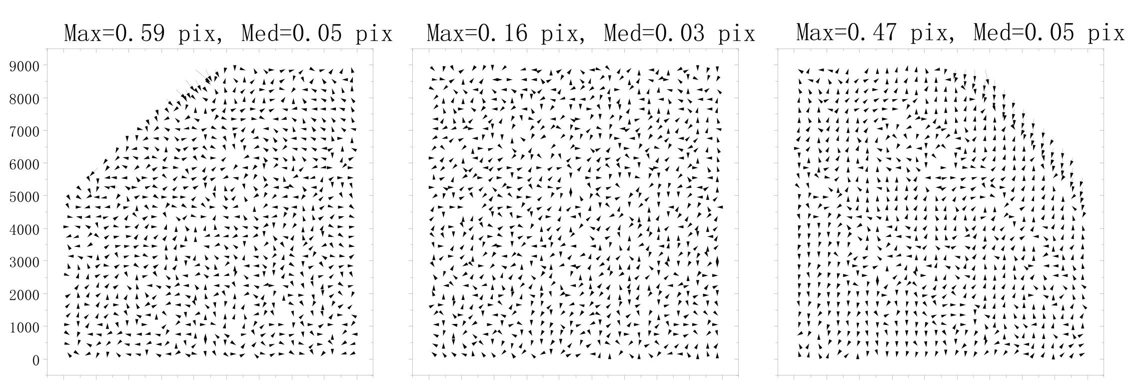

Continued on next page

CSTR: 32290.14.JUSTC-2024-0124
DOI: 10.52396/JUSTC-2024-0124
JUSTC, **2025**, 55(4): 0402

Continued from previous page

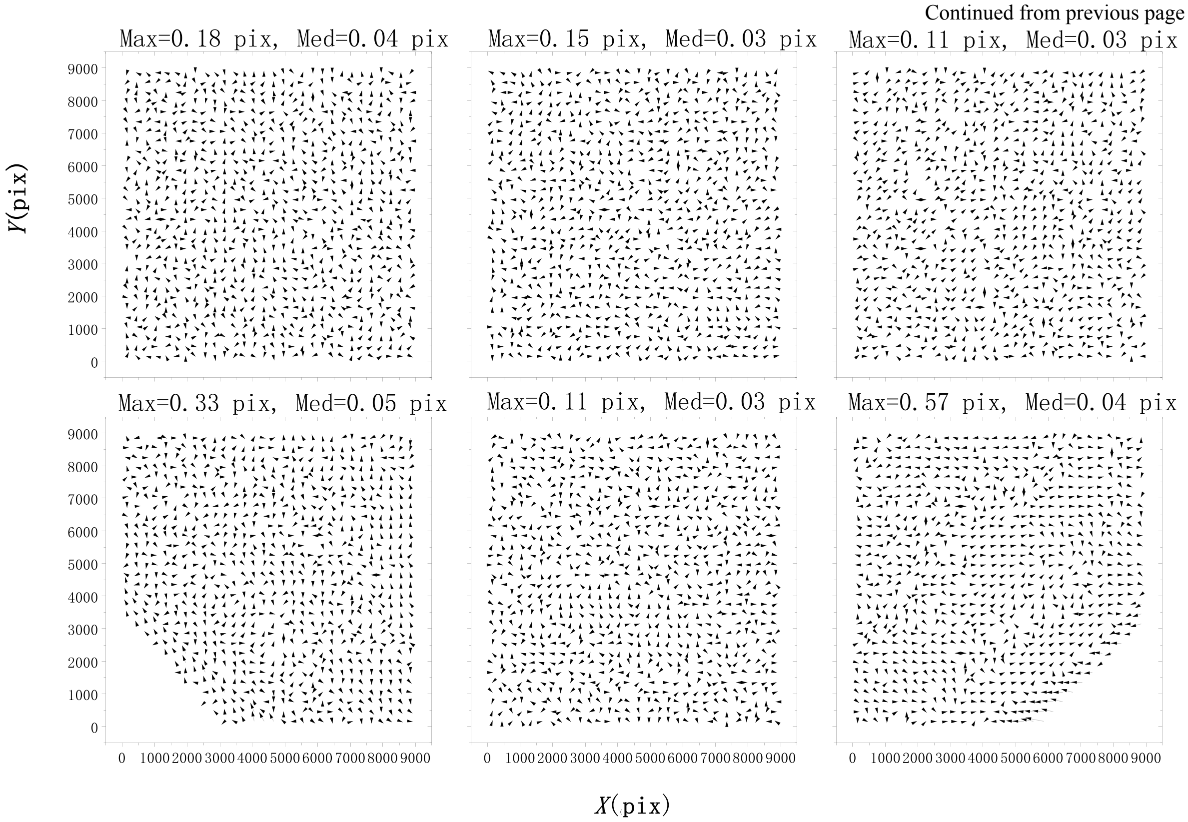

Fig. 7. The remains residuals after geometric distortion (GD) for the P0−P8 chips. The magnitude of each vector is exaggerated by a factor of 1000.

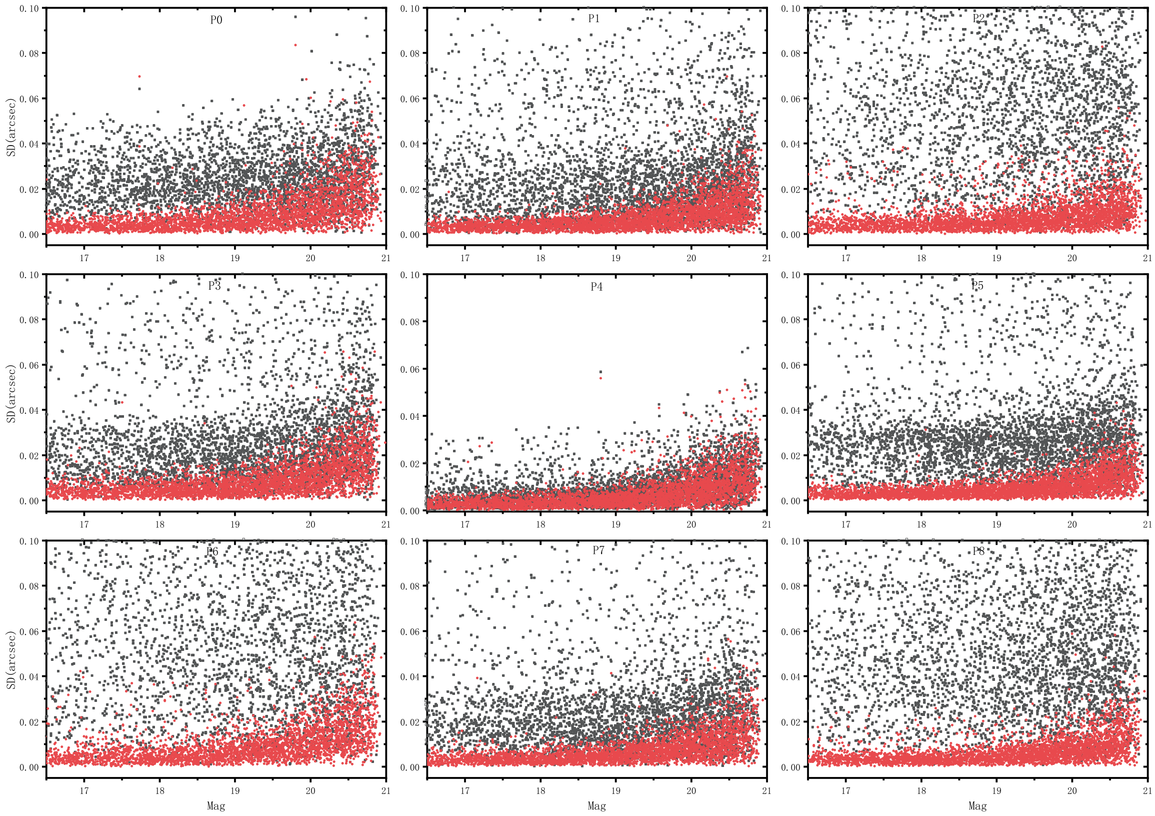

Fig. 8. The distribution of standard deviation (SD) for WFST, with the red points representing SD after distortion correction and the black points indicating SD before distortion correction. The SD is corresponding to two directions in form of $\sqrt{(\sigma_\alpha \cos\delta)^2 + \sigma_\delta^2}$. σ_α is the SD in right ascension (RA), σ_δ is the SD in declination (DEC), and σ_δ is the declination of the object.

CSTR: 32290.14.JUSTC-2024-0124
DOI: 10.52396/JUSTC-2024-0124
JUSTC, **2025**, 55(4): 0402

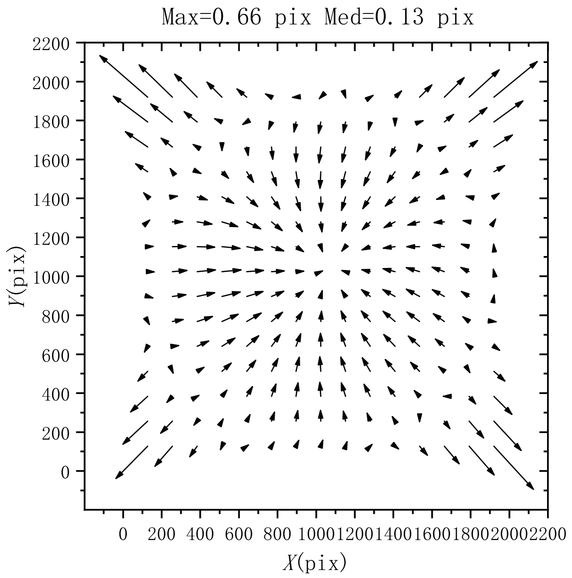

Fig. 9. Geometric distortion (GD) for the YAHPT. The magnitude of each vector is exaggerated by a factor of 200.

pixel coordinate of each chip. (b) The projection center is the point of each chip and the center pixel coordinate of each chip without considering gap size. (c) The projection center is the point of chip P4 and the center pixel coordinate of the fourth chip, accounting for gap size. The results of the calculations for the three cases are displayed in Fig. 12. While the variation among the three cases is minimal, as a systematic error, it is necessary to select the results from Table 4 to achieve high precision. Additionally, inaccurately selecting the projection center can introduce new distortions.

3 Discussions and conclusions

The WFST is designed primarily for the analysis of large sky surveys. To guarantee the precision of the astrometric data, calibrating the relevant parameters via an astrometric model is essential. The parameters of the astrometric model are calibrated using the GD values and gaps. We analyzed the GD for the WFST via photographic astrometry imaging. Our investigation reveals that the median GD values for different chips of WFST range from 0.25 pixels to 2.22 pixels. The distribution aligns with the optical design (based on internal report

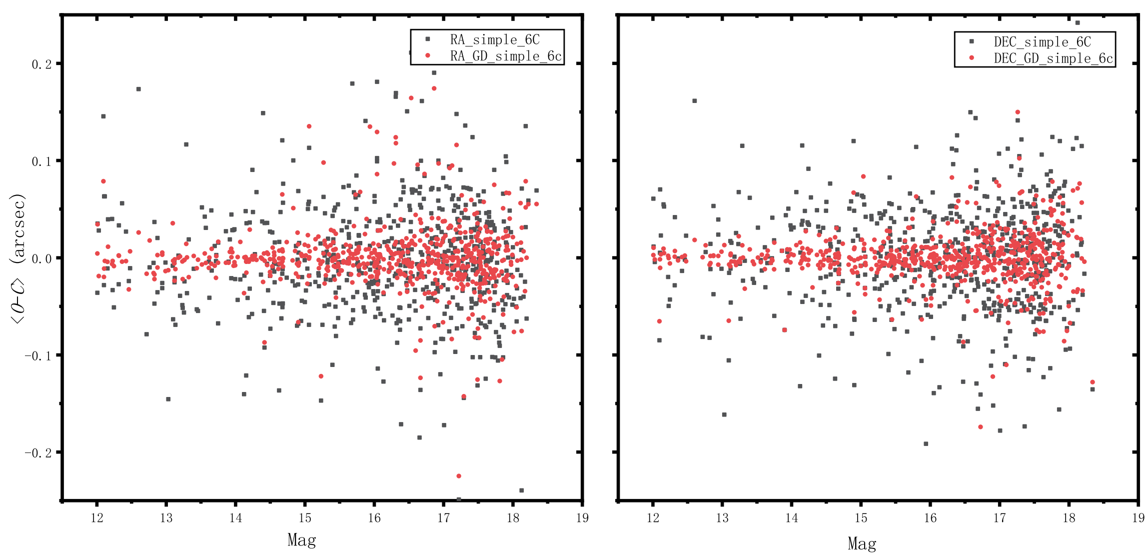

Fig. 10. The distribution of residuals for the YAHPT is shown, with the red points representing residuals after distortion correction and the black points indicating residuals before distortion correction.

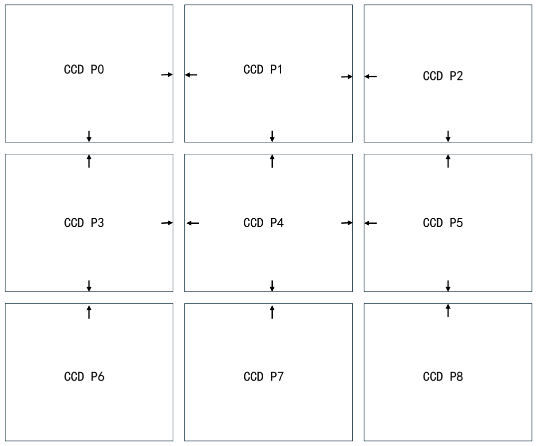

Fig. 11. The chip’s arrangement of WFST.

Table 3. The gap and parallelism of the WFST.

Gaps	Mean (mm)	Mean std (mm)	Angle (°)	Angle std (°)
P0,P1	4.935	0.035	0.088	0.053
P1,P2	4.935	0.036	0.088	0.053
P0,P3	4.931	0.041	0.058	0.039
P1,P4	4.927	0.035	0.062	0.050
P2,P5	4.689	0.029	0.359	0.060
P3,P4	4.699	0.034	0.203	0.067
P4,P5	4.991	0.037	0.046	0.050
P3,P6	4.843	0.024	0.051	0.047
P4,P7	7.765	0.040	0.069	0.038
P5,P8	5.035	0.029	0.086	0.053
P6,P7	1.947	0.047	0.108	0.061
P7,P8	1.922	0.030	0.053	0.039

CSTR: 32290.14.JUSTC-2024-0124
DOI: 10.52396/JUSTC-2024-0124
JUSTC, **2025**, 55(4): 0402

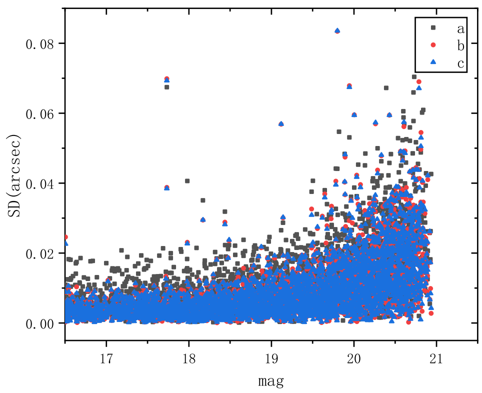

Fig. 12. The standard deviation (SD) of the stars is calculated under three different scenarios: (a) The projection center is determined by the pointing direction of each chip and the center pixel coordinate of each chip. (b) The projection center is based on the pointing direction of each chip and the center pixel coordinate of chip P4, disregarding gap size. (c) The projection center is derived from the pointing direction of the chip P4 and the center pixel coordinate of the chip P4, taking into account the size of the gap.

Table 4. In various chip coordinate systems, the pixel coordinates of the center of the chip P4.

	CRPIX1	CRPIX2
P0	14317	−5109
P1	4608	−5108
P2	−5107	−5085
P3	14310	4616
P4	4608	4616
P5	−5107	4616
P6	14019	14624
P7	4608	14624
P8	−4800	14624

CRPIX1 and CRPIX2 are the pixel coordinates of the projection center.

data). This also validates the correctness of the GD solution method. GD correction is most effective when the six-constant model is used. After applying the GD correction, the precision of the WFST reaches 4 mas. However, for Fig 4, even after distortion correction (red points), the (O−C) values are not evenly distributed on both sides of the zero mean, particularly in the right ascension. Similarly, for Fig. 5, the standard deviation in the declination is clearly worse than that in right ascension. This may be due to factors such as differential color refraction and/or the charge transfer efficiency of the CCD, suggesting that additional observation data may be needed for future confirmation and analysis after the WFST upgrade.

Then we solve the gap issues among WFST chips via photographic astrometry. This process allows us to determine more precise CRPIX1 and CRPIX2 parameters for each chip relative to the center of chip P4, accounting for the gaps between them. These calibrated parameters are prerequisites for obtaining an astrometric solution for WFST. It is anticipated that the calibration model will remain applicable in the future as the WFST undergoes further updates.

Acknowledgements

This work was supported by the Strategic Priority Research Program of the Chinese Academy of Sciences (XDA0350300), the National Natural Science Foundation of China (12203105, 12103091, 62394351, 12073008). We acknowledge the science research grants from the China Manned Space Project (CMS-CSST-2021-A12, CMS-CSST-2021-B10).

Conflict of interest

The authors declare that they have no conflict of interest.

Biographies

Yuxi Jiang is a graduate student at the University of Science and Technology of China. Her research mainly focuses on high-precision astrometry of the solar system.

Fan Li is a Senior Engineer at the Purple Mountain Observatory of the Chinese Academy of Sciences. He received his Ph.D. degree from the University of Chinese Academy of Sciences in 2020. His research mainly focuses on the dynamics of the solar system and the ephemerides of the solar system objects.

Xin Wang is a Researcher at the Purple Mountain Observatory of the Chinese Academy of Sciences. He received his Ph.D. from the Department of Astronomy at Nanjing University in 2003. His research mainly focuses on the spacecraft orbital mechanics and the detection methods for space objects and debris.

References

[1] Deng L, Yang F, Chen X, et al. Lenghu on the Tibetan Plateau as an astronomical observing site. *Nature*, **2021**, *596*: 353–356.
[2] Wang T, Liu G, Cai Z, et al. Science with the 2.5-meter Wide Field Survey Telescope (WFST). *Science China Physics*. *Mechanics & Astronomy*, **2023**, *66*: 109512.
[3] MPC. MPEC 2023-W83: 2023 WB2. **2023**. https://minorplanetcenter.net/mpec/K23/K23W83.html. Accessed July 01, 2024.
[4] MPC. MPEC 2023-W102: 2023 WK2, **2023**. https://www.minorplanetcenter.net/mpec/K23/K23WA2.html. Accessed July 01, 2024.
[5] MPC. MPEC 2023-W79: 2023 WX1, **2023**. https://minorplanetcenter.net/mpec/K23/K23W79.html. Accessed July 01, 2024.
[6] Bellm E C, Kulkarni S R, Barlow T, et al. The Zwicky Transient Facility: Surveys and scheduler. *Publications of the Astronomical Society of the Pacific*, **2019**, *131*: 068003.
[7] Ye Q, Masci F J, Ip W-H, et al. A twilight search for atiras, vatiras, and co-orbital asteroids: Preliminary results. *The Astronomical Journal*, **2020**, *159*: 70.
[8] Wiegert P, Innanen K, Mikkola S. Earth Trojan asteroids: A study in support of observational searches. *Icarus*, **2000**, *145*: 33–43.
[9] Mróz P, Otarola A, Prince T A, et al. Impact of the SpaceX Starlink satellites on the Zwicky Transient Facility survey observations. *The Astrophysical Journal Letters*, **2022**, *924*: L30.
[10] Yuan Y, Li F, Fu Y, et al. New precise positions in 2013–2019 and a catalog of ground-based astrometric observations of 11 Neptunian satellites (1847–2019) based on *Gaia*-DR2. *Astronomy & Astrophysics*, **2021**, *645*: A48.
[11] Yuan Y, Li F, Fu Y, et al. The orbits of Triton and Nereid and the pole orientation of Neptune from Voyager, *Hubble* Space Telescope,

CSTR: 32290.14.JUSTC-2024-0124
DOI: 10.52396/JUSTC-2024-0124
JUSTC, **2025**, 55(4): 0402

and Earth-based astrometry in 1847–2020. *Astronomy & Astrophysics*, **2021**, *654*: A66.

[12] Guo B, Peng Q, Chen Y, et al. The astrometric performance test of 80 cm telescope at Yaoan Station and precise CCD positions of apophis. *Research in Astronomy and Astrophysics*, **2022**, *22* (5): 055007.

[13] Shang Y J, Peng Q Y, Zheng Z J, et al. New CCD astrometric observations of Himalia using Gaia DR2 in 2015–2021. *The Astronomical Journal*, **2022**, *163* (5): 210.

[14] Yuan Y, Li F, Fu Y, et al. Reconciling results of 2019 and 2020 stellar occultations on Pluto's atmosphere. *Astronomy & Astrophysics*, **2023**, *680*: A9.

[15] Peng Q Y, Guo B F, Vienne A, et al. CCD astrometric measurements for the dwarf planet Haumea by ground-based telescopes. *Astronomy & Astrophysics*, **2023**, *672*: A61.

[16] Li F, Yuan Y, Fu Y, et al. Dynamical masses of 20 asteroids determined with Gaia DR3 asteroid observations. *The Astronomical Journal*, **2023**, *166*: 93.

[17] Li F, Yuan Y, Fu Y. Ephemeris development for asteroids 35633 and 135356 and their orbital evolution induced by a close encounter. *SCIENTIA SINICA Physica*. *Mechanica & Astronomica*, **2021**, *51*: 029502.

[18] Anderson J, King I R. An improved distortion solution for the *Hubble Space Telescope*'s WFPC2. *Publications of the Astronomical Society of the Pacific*, **2003**, *115*: 113–131.

[19] Anderson J, Bedin L R. Ground-based CCD astrometry with wide field imagers. I. Observations just a few years apart allow decontamination of field objects from members in two globular clusters. *Astronomy and Astrophysics*, **2006**, *454* (3): 1029–1045.

[20] Bellini A, Bedin L R. Ground-based CCD astrometry with wide field imagers. IV. An improved geometric-distortion correction for the blue prime focus camera at the LBT. *Astronomy and Astrophysics,*, **2010**, *517*: A34.

[21] Wang N, Peng Q Y, Zhou X. A distortion solution for the Bok telescope with four CCD chips. *Monthly Notices of the Royal Astronomical Society*, **2019**, *485* (2): 1626–1634.

[22] Zheng Z J, Peng Q Y, Vienne A, et al. A deeper solution to the actual geometry of CCD mosaic chips. *Astronomy & Astrophysics*, **2022**, *661*: A75.

[23] Rodeghiero G, Pott J U, Massari D, et al. Towards an overall astrometric error budget with MICADO-MCAO. arXiv: 1902.00933, **2019**.

[24] Bertin E, Arnouts S. SExtractor: Software for source extraction. *Astronomy and Astrophysics Supplement Series*, **1996**, *117*: 393–404.

[25] Gaia Collaboration. Gaia Early Data Release 3. Summary of the contents and survey properties. *Astronomy and Astrophysics*, **2021**, *649*: A1.

CSTR: 32290.14.JUSTC-2024-0124
DOI: 10.52396/JUSTC-2024-0124
JUSTC, **2025**, 55(4): 0402